EUROFUSION WPDTT2-CP(16) 15303

M Poradzinski et al.

Integrated Core-SOL-Divertor Modelling for DEMO with Tin Divertor

Preprint of Paper to be submitted for publication in Proceedings of 29th Symposium on Fusion Technology (SOFT 2016)

This work has been carried out within the framework of the EUROfusion Consortium and has received funding from the Euratom research and training programme 2014-2018 under grant agreement No 633053. The views and opinions expressed herein do not necessarily reflect those of the European Commission.

Integrated Core-SOL-Divertor Modelling for DEMO with Tin Divertor

M. Poradziński, I. Ivanova-Stanik, G. Pełka, R. Zagórski

Institute of Plasma Physics and Laser Microfusion, Hery str. 23, 01-497, Warsaw, Poland

Abstract

This paper analyzes a possible operational space for the DEMO device with the tin divertor. The simulation is performed with the COREDIV code which self-consistently solves core and scrape-off layer transport equations for plasma and impurity. A simple model of divertor surface evaporation was included in the code. The simulation was performed for the DEMO 1 April 2015 configuration. Influence of the sputtering, prompt redeposition and evaporation of the liquid tin divertor was taken into account. Simulation without impurity seeding shown that plasma in DEMO with the tin divertor is characterized with higher than 80% radiation fraction, and 55MW of power to the plate. Power across the separatrix stays below the L-H threshold. In spite of high radiation fraction seeding with additional impurity is necessary to reduce the power to the divertor targets to acceptable levels. In presence of the argon seeding power to the plate is reduced to 23 MW, power across the separatrix reaches 150MW which is compatible with the H-mode operation.

Keywords: DEMO, Liquid Metal Divertor, impurity, edge plasma

1. Introduction

DEMO will be a tokamak that follows ITER on the way to commercial fusion. Construction of DEMO faces many challenges. The device is expected to operate in the H-mode, which carries the necessity of power to scrape-off layer (SOL) value above the L-H threshold. On the other hand it is postulated that the divertor power load cannot exceed 5MW/m^2 [1]. In other words, plasma in the SOL needs to be cold enough so that the divertor stands the heat. Cooling plasma can be achieved by seeded or by intrinsic impurities i.e. particles originating from the divertor.

Liquid Metal (LM) divertor is considered as an alternative to a standard tungsten (W) one. Self-replenishing liquid surfaces would eliminate some issues such as melting and re-crystallization that could degrade solid PFCs [3]. A LM divertor can be realized via capillary porous system (CPS) which consists of a mesh in which liquid metal flows. Beneath the mesh a liquid metal reservoir is located. It allows to replenish liquid metal losses due to sputtering and vaporisation. A CPS considered in a LM divertor stabilizes the surface and supresses withdrawing the liquid metal droplets to the SOL region by $j \times B$ forces. A CPS scheme for a liquid devertor has proven to be the most promising configuration to confine liquid metal against MHD effects, by means of capillary forces [5].

Liquid tin (Sn, Z=50) is one of the promising candidates for LM divertor due to its low melting point (see Tab. 1) and low vapor pressure [4]. Low Sn threshold energy for D and T sputtering (see Fig. 1.) leads to Sn impurity content in the SOL, which in turn increases the Sn concentration even more as a result of low energy threshold for self-sputtering. As a consequence, high impurity radiation close to the divertor decreases the operation plasma temperature and leads to semi-detached or detached conditions in the divertor. Achieving semi-detached conditions is much harder in case of a tungsten divertor. Tungsten high threshold energy for D and T sputtering prevents from releasing the element to the SOL at lower temperatures. Additonally tungsten radiation at lower energies is much lower (see Fig. 2.) than tin and achieving a semi-detached regime requires additional seeding [2].

	W	Sn
Atomic number	74	50
Melting point, °C	3422	231.93
Boiling point, °C	5930	2602
Thermal conductivity at 500 °C, W/m/K	127.0	35.8
Heat of evaporation, kJ/mol	806.7	296.1

Table 1: Tin and tungsten physical properties.

The aim of this analysis is to find a possible operational space for DEMO 1 with the Sn divertor setup. Influence of the sputtering, prompt redeposition and evaporation of the liquid Sn divertor is taken into account.

2. Modelling approach

Since the energy balance in tokamaks with metallic walls depends strongly on the coupling between the bulk and

Email address: michal.poradzinski@ipplm.pl (M. Poradziński)

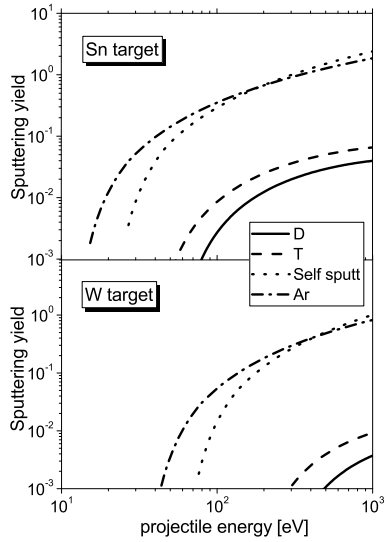

Figure 1: Sputtering yield.

the scrape-off layer (SOL) plasma, modelling requires the transport problem to be addressed in both regions simultaneously. The above statement applies also to a liquid tin divertor because tin radiates both in the core and in the SOL (see Fig. 2.). The simulation was performed with

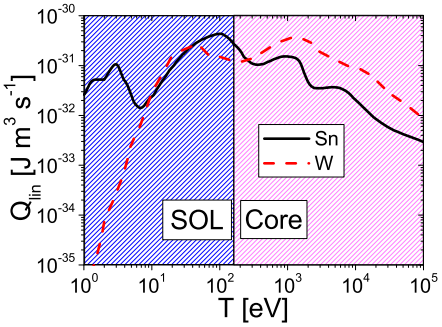

Figure 2: Corona cooling rate.

the COREDIV code [6] which self-consistently solves 1D radial transport equations of plasma and impurities in the core region and 2D multi-fluid transport based on Braginskii equations in the scrape-off layer region. The code has been successfully benchmarked with a number of JET discharges, including the nitrogen and neon seeded JET ILW configuration [7]. COREDIV has also been applied to ASDEX discharges in the full W environment [8]. The physics model used in the COREDIV code is relatively complex and has been already presented elsewhere [9, 10], however we point out some elements of the model which are important for the present study. Densities of main plasma and impurity ions are given by the solution of the radial diffusion equations with diffusion coefficients $D_i = 0.35\chi_e$ and small anomalous pinch term $W_i (= W_j^k$ the same for all species). For all ions, background plasma and impurities, we have used the same anomalous transport coefficient defined by: $D_i^{an} = 0,35\chi_{e,i}^{an}$, $V_i^{pinch} = C_p \left(\frac{\tau_e}{2.8}\right)^2 D_i^{an} \frac{r}{a^2}$, where C_p is the density peaking coefficient and $C_p = 0.5$ for main plasma ions has been chosen as a reference value in our simulations. This results in the ratio between central and average electron density being equal to about 1.3 $\frac{n_e(0)}{\langle n_e \rangle_{vol}} \sim 1.3$. For impurities, an optimistic assumption is used with $C_p = 0$ (no impurity pinch) for the reference simulations. We note, that our assumption is consistent with the experiments on the ASDEX-Upgrade, where the ECRH control of the central electron temperature leads to mitigation of W accumulation in the core [11]. The SOL region is approximated by a simple slab geometry (poloidal and radial direction) with classical transport in the poloidal direction and anomalous transport in radial direction using the following transport coefficients $D_i = \chi_i = 0.5\chi_e$. Similarly as, in the core part of the model, it is assumed that for all ions the anomalous transport is the same and they have the same temperature. We used for the value of radial anomalous transport in the SOL $D_{rad}^{SOL} = 0.5m^2/s$.

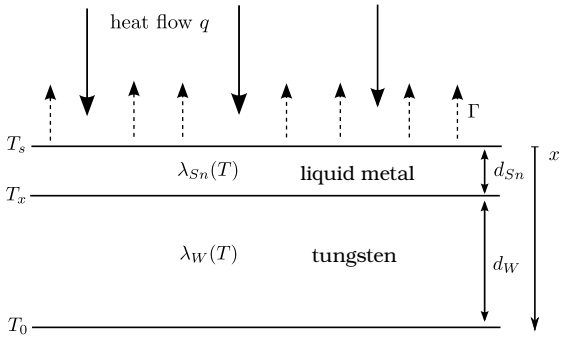

Figure 3: Liquid metal divertor scheme.

Main sources of tin in the plasma are sputtering and evaporation of the divertor plate. Specifically for the simulations of the LM divertor we included in the code a simple model of divertor surface evaporation. A LM divertor scheme is presented in Fig. 3, where d_{Sn} and d_W are a liquid metal layer and a tungsten layer thicknesses respectively. Their thermal conductivities are $\lambda_i(T)$, i=Sn,W (see Table 1. for reference values at 500°C). Coolant temperature T_0 and the heat flux q are given. T_x and T_s are the layers contact surface temperature and the LM surface temperature respectively. A flux of particles $\Gamma\,[\mathrm{m}^{-2}\mathrm{s}^{-1}]$ leaving the divertor surface is given by the Hertz-Knudsen equation:

$$\Gamma = \frac{p_{sv}}{\sqrt{2\pi k_B m T_s}}, \tag{1}$$

where p_{sv} (saturated vapor pressure) is given by [13]:

$$\log_{10}\left(\frac{p_{sv}}{p_{atm}}\right) = 5.262 - 15332/T_s, \tag{2}$$

where $p_{atm} = 1013\mathrm{hPa}$. Temperatures T_x and T_s are found from the solution of the 1D equation $q = -\lambda(T)\frac{dT}{dx}$. Thermal conductivity dependence on the temperature T was

extracted from the tables [14]. A linear function was fitted to the λ data. The latent heat of evaporation is neglected in the model. For maximum vaporization rates of the order of 10^{21}-$10^{22}\,\mathrm{s}^{-1}$, such that still do not cause disruption, the latent heat of evaporation released is $\sim$ 5kW which is around 0.5% of the local heat flux to the divertor ($\sim$ 1MW/m^2). Influence of the coolant tempera-

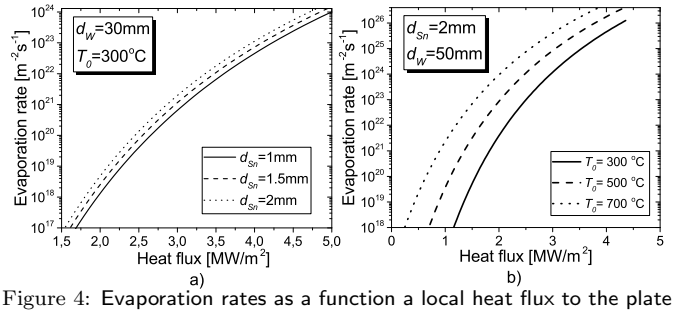

Figure 4: Evaporation rates as a function a local heat flux to the plate for $d_Sn = 2mm$ and $d_W = 50mm$ for coolant temperatures $T_0 = 300°C, 500°C, 700°C$

.

ture T_0 and tungsten layer thickness on the evaporation is shown in Figs. 4. Increase of the W layer width leads to strong reduction of the critical heat flux. In case of $d_W = 50$mm and $d_{Sn} = 2$mm evaporation rate of the size of $10^{22}\,\mathrm{m}^{-2}\mathrm{s}^{-1}$ is achieved already at the local heat flux level of $2.2\,\mathrm{MeV/m}^2$ whereas in the case of $d_W = 30$mm the same evaporation rate requires heat flux of the level of $3.4\,\mathrm{MeV/m}^2$. One can observe in Fig. 4. a) that the evaporated flux is reduced with the thickness of the Sn layer. Reduction of the local heat flux to the target is achieved by tilting the divertor with respect to the magnetic flux.

3. Simulation

The simulations were performed according to the European DEMO 1 April 2015 configuration with the following main parameters [12]: toroidal radius $R_T = 9.073$m, minor plasma radius $a = 2.926$m, plasma current $I_pp = 19.6$MA, toroidal magnetic field $B_T = 5.667$T, elongation $\varepsilon = 1.56$, volume averaged electron density $\langle n_e \rangle_{\mathrm{VOL}} = 0.933 \times 10^{20}\mathrm{m}^{-3}$, separatrix density $n_{es} = 40\% \langle n_e \rangle_{\mathrm{VOL}}$, H-factor (IPB98(y,2)) $H98 = 1.1$ and auxiliary heating power P_{aux} equal to 50 MW.

3.1. Dependence on the coolant temperature

Four points of temperature $T_0 = 100$°C, 300 °C ,500 °C and 700 °C were chosen for the simulation. Tin layer width was set to $d_{Sn} = 2$mm and tungsten base width is set to $d_W = 50$mm.

Magnetic field surface inclination w.r.t. divertor was set to 13.5° so that effectively the magnetic field lines hit the divertor with 3° angle. Result of the simulation in form of basic plasma parameters is given in Table 2. Increasing of the coolant temperature level has no effect on the P_α and Q. The power across the separatrix P_{SOL} is below the

T_0[°C]	100	300	500	700
P_α[MW]	396.4	393.7	393.1	391.9
P_{plate}[MW]	52.8	47.0	38.1	28.0
P_{SOL}[MW]	124.1	119.2	124.3	119.9
Q	39.6	39.4	39.3	39.2
T_e^{plate}[eV]	3.6	3.1	2.6	1.95
$\Gamma_{sputt}[\times 10^{21}\mathrm{s}^{-1}]$	6.2	5.3	3.8	2.6
$\Gamma_{vap}[\times 10^{21}\mathrm{s}^{-1}]$	0.39	1.8	3.7	6.2
c_{Sn}[%]	0.055	0.055	0.054	0.054
f_{rad}	0.853	0.865	0.854	0.868

Table 2: Plasma parameters for different coolant temperatures T_0. The simulation was performed for $d_W = 50$mm, $d_{Sn} = 2$mm.

L-H threshold which is 132.8 MW according to the scaling laws [15]. Evaporation is dominant for $T > 500$ °C. For $T > 500$ °C power to the plate is lower than 40MW. Sn concentration in the core does not exceed 0.06%. Low value of P_{SOL} is due to tin radiation in the core. Increase of P_{SOL} can be achieved by seeding impurity which enhances the radiation in the SOL and therefore further reduce target power load but radiates subdominantly in the core. Above conditions are satisfied by Ar (Z=18) and therefore this element was chosen as seeded impurity in the simulation.

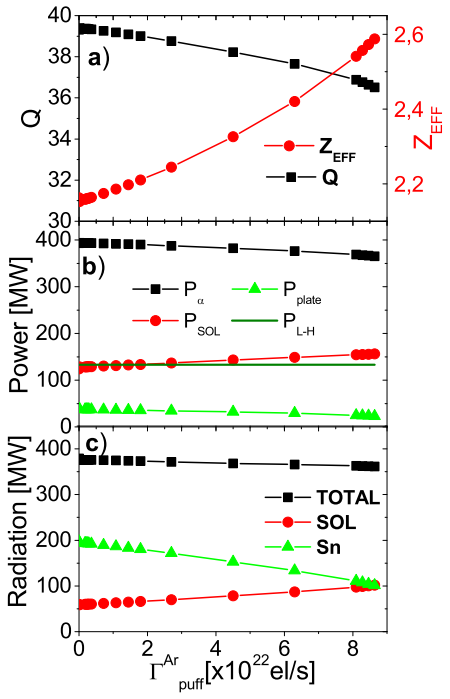

Figure 5: Plasma parameters dependence on Γ^{Ar}_{puff}

3.2. Influence of the Ar seeding

Key plasma parameters dependence on Ar gas puff (Γ^{Ar}_{puff}) is depicted in Figs. 5. For large Γ^{Ar}_{puff} ($> 2.5 \times$

10^{22} el/s) P_{SOL} exceeds L-H threshold (132.8 MW) entering the H-mode operation space. As a result of Ar seeding a slight reduction of the total radiation is observed. In spite of that the total radiation fraction slightly increases and exceeds 85%. This is mainly due to decrease of P_α caused by plasma dilution in the core. Nevertheless Q factor drops down only by about 4%. Tin radiation is a small fraction of the total radiation in the center of the core as

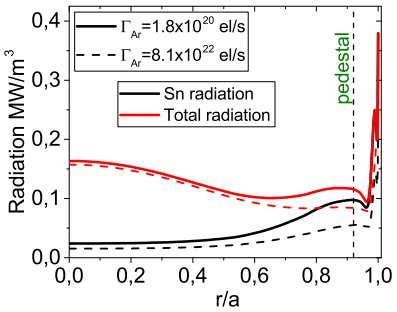

Figure 6: Sn radiation profiles.

can be observed in Fig. 6. However it contributes dominantly in the pedestal region independently on the gas puff level which can result in the pedestal degradation and affect energy confinement.
Sn radiation in the SOL constitutes to 50% of the SOL radiation at low seeding and 20% at high Ar seeding. Reduction of the Sn radiation in the SOL is surpassed by increase of Ar radiation and causes reduction of the target plate power load (P_{plate}) down to 23 MW. This allows for the development of the semi-detached or detached plasma in the divertor region ($T_e^{plate} < 2$eV).

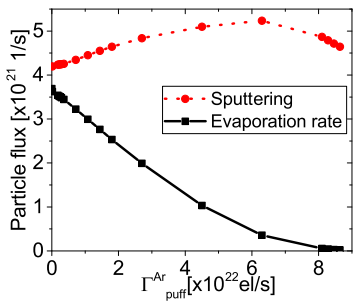

Figure 7: Sputtering and evaporation rates dependence on the argon seeding Γ^{Ar}_{puff}.

In the absence of Ar seeding sputtering and vapor flux from the divertor contribute equally to the particle flux originating from the divertor. With the gas puff increase vaporization drops down whereas sputtering yield stays at the same level. At high gas puff, in the semi-detached regime vaporization is negligible (Fig. 7.) Due to low T_e^{plate} prompt redeposition has no infuence on the plasma.

4. Conlusions

The self-consistent (core-edge) COREDIV code has been used to analyze DEMO with liquid divertor (Sn) including model of evaporation and argon seeding. In the absence of seeding power crossing the separatrix stays below the L-H threshold. Simulation with argon seeding shows that P_{SOL} slightly exceeds L-H threshold. Seeding by medium Z impurities (Ar) leads to additional radiation in the SOL region allowing for T_{plate} reduction below 2 eV and simultaneous strong reduction of the heat load (< 23 MW). Since the threshold temperature (T_{th}) for Sn sputtering is relatively low (5-6 eV), the conditions at the divertor are such that plasma temperature stays close to T_{th} leading to semi-detached or detached conditions in the divertor. Prompt re-deposition has no influence on the working point. Possibility of the degradation of the energy confinement by Sn might be a problem, since the Sn radiation is localised in the pedestal region. Liquid tin could be a viable solution for the target materials.

Acknowledgements

This work has been carried out within the framework of the EUROfusion Consortium and has received funding from the Euratom research and training programme 2014-2018 under grant agreement No 633053. The views and opinions expressed herein do not necessarily reflect those of the European Commission. This scientific work was partly supported by Polish Ministry of Science and Higher Education within the framework of the scientific financial resources in the year 2016 allocated for the realization of the international co-financed project.

References

[1] Zohm H. *et al.* Nucl. Fusion **53** 073019 (2013)
[2] R. Zagórski, *et al.*, *Fusion Eng. and Design* **109-111** 37-41 (2016)
[3] R.E. Nyrgen, F.E. Tabarés, *Nuclear Materials and Energy* **9**, 6-21, (2016)
[4] J.W. Coenen ,*et al.* , *Phys. Scripta* **T159**, 014037, (2014)
[5] Ono M. United States: Nova Scientific Publications (August 2012), 2012. Web. doi:10.2172/1056493.
[6] R. Zagórski, *et al.*, *Nucl. Fusion*, **53**, 073030 (2013)
[7] R. Zagórski, *et al.*,, *J. Nucl. Mater.* **463**, 649653 (2015)
[8] K. Gałązka, *et al.*, *Contrib. Plasma Phys.* **56**, No. 6-8, 772 777 (2016) DOI: 10.1002/ctpp.201610008
[9] R. Zagórski, *et al.*, *J. Nucl. Mater.* **404**, 390-391 (2015)
[10] G. Telesca, *et al.*, *J. Nucl. Mater.* **438** (Supplement), S567 (2013)
[11] R. Neu, *et al.*, *Nucl. Fusion*, **45**, 209 (2005)
[12] R. Kemp, *et al.*, EFDA Report WP11-SYS-01-ACT5 (2012).
[13] C. B. Alcock, V. P. Itkin and M. K. Horrigan, *Canadian Metallurgical Quarterly* 1984; **23**(3), 309-313. DOI: 10.1179/cmq.1984.23.3.309
[14] C. Y. Ho, R. W. Powell and P. E. Liley, *J. Phys. Chem. Ref. Data* **1**, 279 (1972). DOI: 10.1063/1.3253100
[15] Y. R. Martin, *et al.*, *Journal of Physics: Conf. Series* 123, 012033 (2008)